SAND96-0460C
CONF-960543--19

HIGH-ACCURACY TIME- AND SPACE-RESOLVED STARK SHIFT MEASUREMENTS

J.E. Bailey, R. Adams, A.L. Carlson, C. H. Ching, A.B. Filuk, and P. Lake

Sandia National Laboratories, Albuquerque, N.M., 87175-1196

Stark-shift measurements using emission spectroscopy are a powerful tool for advancing understanding in many plasma physics experiments. We use simultaneous 2-D-spatial and time-resolved spectra to study the electric field evolution in the 20 TW Particle Beam Fusion Accelerator II ion diode acceleration gap. Fiber optic arrays transport light from the gap to remote streaked spectrographs operated in a multiplexed mode that enables recording time-resolved spectra from eight spatial locations on a single instrument. Design optimization and characterization measurements of the multiplexed spectrograph properties include the astigmatism, resolution, dispersion variation, and sensitivity. A semi-automated line-fitting procedure determines the Stark shift and the related uncertainties. Fields up to 10 MV/cm are measured with an accuracy $\pm$ 2-4%. Detailed tests of the fitting procedure confirm that the wavelength shift uncertainties are accurate to better than $\pm$ 20%. Development of an active spectroscopy probe technique that uses laser-induced fluorescence from an injected atomic beam to obtain 3-D space- and time-resolved measurements of the electric and magnetic fields is in progress.

I. Introduction

Visible-light plasma spectroscopy is a powerful diagnostic tool for many applications, including magnetic fusion, inertial confinement fusion, and plasma processing. A common problem in these

DISCLAIMER

experiments is the need for simultaneous time, space, and spectral resolution. This paper describes techniques developed to obtain high-accuracy measurements of Stark-shifted Li I 2s-2p emission from the acceleration gap of the 20 TW Particle Beam Fusion Accelerator II (PBFA II) ion diode, with 1-nsec time resolution and 2-mm, two-dimensional (2-D) space resolution. The Stark shift is used to determine the magnitude of the accelerating electric field[1], while the line intensity and width provide information about the ion beam divergence[2] Measurements of the electric field distribution are combined with the Poisson equation to obtain the charged-particle distribution in the acceleration gap, a key feature for understanding the physics of ion beam generation[1,3]. The measurements can also be compared with computer simulations[4] as a means of evaluating the simulation fidelity. In addition, the small field components transverse to the acceleration direction that deflect the ion beam and decrease the beam brightness can be determined from high-accuracy 2-D measurements of the magnitude of the total electric field vector[5].

II. Experiment

The geometry of the cylindrically-symmetric applied-magnetic-field PBFA II ion diode[6,7] is shown in Figure 1. PBFA II supplies a 20 TW, 20 nsec, 10 MV power pulse through conical magnetically-insulated transmission lines connected to the top and bottom of the diode. An approximately 3 T magnetic field, applied parallel to the anode, insulates the anode-cathode (AK) gap against electron losses. The lithium ion beam is accelerated radially inward from the inner surface of a 17-cm-radius cylindrical anode, through a virtual cathode composed of electrons trapped in the magnetic field, and onto a target placed at the axis. The acceleration gap is typically 20 mm. Lithium neutral atoms are injected in the gap when lithium-beam ions undergo charge exchange

near the anode surface. The Li I 2p population density in the gap reaches ~ 0.5-5 $x10^{12}$ cm^{-3}, providing about 0.13 - 1.3 x 10^{12} atoms emitting in a typical spectroscopy line-of-sight volume. We collect the 2s-2p emission from these atoms using a 2-D array of 100-μm-diameter fiber optics imaged using a 16-mm focal-length lens and a magnification of about 15. The spatial resolution is about 2 mm because we integrate over the 8 cm height of the anode and the focus degrades near the top and bottom. The alignment accuracy of the line-of-sight-bundle relative to the anode surface is better than ± 0.5mm. The spatial dependence of the absolute collection efficiency is measured as in Reference 8, with a peak value equal to ~$3x10^{-5}$.

The emission is transported about 45 m in the fiber optics to a remote screen room where it is injected into spectrographs. A streak camera located in the exit focal plane of each spectrograph records time-resolved spectra, using an effective photocathode that is 40 mm long and 300 μm tall. High sensitivity is achieved using a microchannel plate (MCP) to intensify the streaked spectral image before it is recorded on Kodak TMAX 400 film. The overall instrument time resolution is limited to about 1 nsec by the bandwidth of the fiber optic, although in our application, low signal intensities often force averaging over 2-4 nsec in order to obtain the desired signal-to-noise ratio. Accurate timing is obtained by recording an pulsed laser diode on each spectrum, combined with optical-time-domain-reflectivity measurements of the fiber lengths and the fiber refractive index. We verified that the timing accuracy among the spatial channels was better than ± 0.4 nsec and the accuracy relative to the electrically-recorded diode diagnostics was better than ±2 nsec.

Simultaneous space- and time-resolved data is obtained by using a multiplexed streaked spectrograph similar to those that have been developed independently at the Joint European Torus[9]

and at Lawrence Livermore National Laboratories[10]. The multiplexing is achieved by mounting eight fiber optics at the spectrograph input, each displaced a few mm in the direction perpendicular to the normal entrance slit. The entrance slit is removed so that each fiber forms a spectrum in the exit focal plane, with each spectrum displaced in the dispersion direction according to the input fiber displacement. Figure 2 illustrates this concept, with a fiber optic displacement in the x direction resulting in a spectrum displaced in the -y direction. A bandpass filter placed at the input prevents the spectra from the different fibers from overlapping. The bandpass filter[11] provides a peak transmission of ~80% with a flat-top profile over 38 Å and a fwhm of ~53 Å. We are, in effect, trading a single spectrograph with ~500 Å range for eight individual spectra with 40 Å range, while preserving the cost and simplicity advantages of a single instrument.

The multiplexed streaked spectrograph design was optimized to maintain the best possible spectral resolution across all the eight channels, while maximizing sensitivity. An important consideration is the astigmatism, defined to be the ratio of the vertical height of the spectrum (measured perpendicular to the spectral dispersion direction) to the input fiber size. Astigmatism potentially results in signal loss because the streak camera photocathode has an active area that is only 300 μm tall. A 1 m Czerny-Turner spectrograph with aspheric hand-polished-master mirrors[12] was used to reduce the astigmatism. A 600 g/mm f/7 grating provided 16.2 Å/mm dispersion. The 100 μm fibers placed at the input without a slit project a ~90 μm fwhm spectral image at the exit focal plane. The MCP intensifier limits the streak camera spatial resolution to about 100 μm, so that the total convolved instrument spectral resolution element is equal to ~134 μm, or 2.2 Å. Each input channel actually uses a 1x3 linear fiber array to enable coupling multiple fibers into a single channel. This offers improved signal levels in experiments where integrating over several spatial chan-

nels does not impact the results.

The effects of input fiber optic displacements on the spectrograph imaging properties were determined in a series of calibration experiments. A 100 μm fiber connected to a low-pressure neon calibration lamp was mounted on an XYZ translation stage at the spectrograph input and spectra corresponding to a variety of input fiber positions were recorded on a CCD camera. We first determined that the displacement of the output spectrum was equal to 1.05 times the input displacement, to within ± 0.4%. Next, the optimum distance from the spectrograph body to the input fiber was measured (y direction in Figure 2), where we define the optimum to be the distance that maintains a spectral resolution element size < 90 μm fwhm. Note that this is a design choice motivated by our desire to maintain spectral resolution across the eight channels, even at the expense of lost signal due to increased astigmatism. Using this information, we designed a fixture that positions the input 1x3 fiber arrays with a 3.7 mm separation between channels and the capability to independantly adjust the input arrays with respect to the spectrograph body. Subsequent measurements were made with the fibers located along the optimum resolution curve. The fwhm of the spectral line in the vertical and spectral directions is shown in Figure 3a. A spectral resolution element fwhm < 90 μm is maintained across the image. The aspheric mirrors render theastigmatism negligible near the nominal slit location, but the vertical fwhm grows as the fibers are displaced. We also measured an ~0.4% variation in dispersion across the total fiber displacement of ± 12 mm, negligible for the experiments reported here. The relative instrument sensitivity is shown as a function of fiber displacement in Figure 3b.The sensitivity of the spectrograph alone decreases near the edges, because for one displacement direction a portion of the light is occulted by the grating after reflection from the focus mirror and, in the other direction, the light misses the

grating after reflection from the collimating mirror. The sensitivity with streak camera detection falls even more for large displacements because of the spectrograph astigmatism.

III. Analysis

A typical streaked spectrum from a PBFA II experiment is shown in Figure 4. In this experiment the line-of-sight configuration shown in Figure 1 was employed, with two multiplexed and two standard streaked-spectrographs recording Li I 2s-2p light from eighteen spatial locations. Wavelength fiducials are applied to each spectrum using a HeNe laser. The analysis of the data begins by digitizing the film. We determined that data recorded with MCP intensifiers must be digitized with a scanning aperture of < 8 μm x 8 μm in order to obtain accurate results. At low light levels the MCP image consists of "dots" superimposed on the film fog background. Each dot is 30-60 μm in diameter (fwhm) and presumably corresponds to a single burst of electrons exiting the MCP wafer to generate phosphor light[13]. The use of a scanning aperture that is larger than the MCP exposure dots results in errors because part of the scan box is elevated to high density (where the dot is) and part is elevated only to the film fog. Due to the logarithmic response of the film, the average exposure over the scanning aperture will be incorrect when the scanning aperture is larger than the MCP exposure dot size and the exposure is so low that the region within the scanning aperture consists of both relatively-high-density MCP dots and essentially un-exposed film. The scanning aperture size must be much less than the MCP dot size in order to avoid this affect.

After the streaked spectrum is digitized we take a temporal sequence of lineouts, typically averaging over 2-4 nsec. A single Gaussian peak is fit to the lines in each lineout as described below.

Fits are performed for the fiducial lines in addition to the LiI 2s-2p lines. We measure the position of the Li I 2s-2p line with respect to the adjacent fiducials. This method compensates for any image distortion in the streak tube / MCP intensifier system.The shift at the time of interest is given by the difference between the position at that time and the position at times after the power pulse when the shift is zero. The uncertainty in the shift is thus a convolution of the uncertainty at the time of interest with the uncertainty in the zero-shift position.

Each spatial channel must be fit at a sequence of 15-20 times. Thus, up to 360 Li I 2s-2p wavelength measurements must be performed to analyze a single experiment. This is done using the ROBFIT line-fitting computer code[14]. The key assumptions in the ROBFIT code are that the data in each pixel is statistically independent of its neighbors and that the data obeys Gaussian statistics. In this context we define a pixel to be a given wavelength interval in a lineout. Averaging over a region large compared to the MCP spatial resolution is required in order to ensure that the signal in each pixel is statistically independent from its neighbors. After the initial digitization with an 8x8 μm aperture, we rebin the data to set the wavelength pixel size equal to 72 μm. We verified that this rebinning results in statistically independent data by determining that rebinning to an even-larger pixel size did not alter the results, and by examining the statistics of the calibration data described below.

The remaining fundamental assumption in ROBFIT is that the data obey Gaussian statistics, equivalent to assuming that the system is dominated by shot noise. For shot noise, the fluctuations in the data are equal to the square root of the number of counts, where in our case a count represents a streak tube photoelectron. Other noise sources that obey different statistics, such as streak

tube scattered electrons, dark current, or MCP self emission, are assumed to be relatively insignificant. In order to investigate the actual statistics of the data and to attain high confidence in the results it was necessary to convert data initially recorded in film exposure units of erg/cm^2 into counts. This is equivalent to relating film exposure to the number of photoelectrons leaving the streak tube photocathode. This is accomplished by measuring the scalefactor (scf) defined such that scf x F= N, where F is the film exposure in erg/cm^2 and N is the number of counts. The scalefactor is determined by recording streaks of a continuum light source that is is roughly constant in time and also in wavelength. Multiple streaks are taken using a range of input power levels. The images were converted from film density to exposure and a set of 10-20 lineouts, each averaging over 4 nsec, were taken from each image. The data from each lineout is nominally at some constant film exposure value, but the signal measured in the individual pixels fluctuates above and below the mean because of shot noise. We assume Gaussian statistics (this is verified below) so that $\sigma^2 = N$, where σ is the standard deviation of the number of counts[15]. The standard deviation of the film exposure is $\sigma_e^2 = \sum_i \{F_i^2 - \langle F\rangle^2\} / (m-1)$, where F_i is the exposure in the i^{th} pixel, $\langle F\rangle$ is the mean exposure, and m is the number of pixels. Using the definition of scf,

$$\sigma_e^2 = \sum_i \{(N_i/scf)^2 - \langle N/scf\rangle^2\} / (m-1) = \sigma^2/scf^2 = N/scf^2$$

and scf = F / σ_e^2. Thus, the scalefactor can be determined by dividing the exposure in the lineout by its variance.The scalefactor depends on the number of photoelectrons required to produce a particular film exposure in one pixel and it thus depends on the lineout duration, the streak tube gain, and the MCP gain. In fact, we are really converting the film exposure into *effective* number of photoelectrons because the gain process itself degrades the signal-to-noise ratio. The ratio of

the signal-to-noise at the photocathode to signal-to-noise at the detector (film) is defined to be the noise factor. Previous measurements[16] indicate that the noise factor for a similar MCP-intensified streak camera is about 2. An additional requirement for the data to obey Gaussian statistics is that the noise factor must be constant as a function of exposure. This is confirmed below.

One way to test the assumption of Gaussian statistics is to plot the signal-to-noise of the data vs. the signal, where the "noise" is defined to be the standard deviation of the data σ and the signal is the exposure expressed in counts, $N = scf \times F$. Since $\sigma = N^{1/2}$ for shot noise, $N/\sigma = N^{1/2}$ and a log-log plot of N/σ vs. N should be straight line with slope 1/2. It is important to note that scf is an average over all exposure values while σ and N refer to a calibration image at some particular input power level. Otherwise, this would be a circular argument, since for each calibration image we derive the scalefactor scf by assuming Gaussian statistics to start with (also note that this test is equivalent to saying that the scale factor is independent of the exposure). The plot shown in Figure 5a indicates not only that shot noise dominates the system, but also that the signal-to-noise ratio is independent of MCP gain over the factor of 2 gain changes typically used in our experiments. The second method for verifying Gaussian statistics is to examine the distribution of the data from a set of lineouts taken from a single calibration image corresponding to one particular mean exposure value. The resulting distributions, after conversion from erg/cm^2 into counts, are displayed in Figure 5b for high and low exposure values. A Gaussian peak is fit to each distribution and the validity of Gaussian statistics is verified by fact that the χ^2 of the fits are close to one[15]. Note that at low exposure values the distribution becomes Poisson, since the fluctuations below the mean value are suppressed as the mean value approaches zero (it is impossible to have negative numbers of counts). The fact that this transition occurs around ~5 counts is additional

evidence that the scalefactor is accurately determined, since this is where the Poisson distribution is expected[15] to become evident.

IV. Error bar accuracy

The use of the electric field data to improve understanding of diode plasma physics rely on confidence that the error bars are a reliable representation of the true uncertainty. For example, comparisons with simulations[1] use the size of the error bars to determine whether any observed differences are statistically significant. In addition, differences of ~10% in the electric field magnitude are found to exist[5] even over a 2 mm azimuthal spacial scale, contrary to the expectation of azimuthal symmetry in an ideal diode. Finally, note that the shift uncertainties are sometimes as low as $\pm$ 0.2 Å. This corresponds to a $\pm$ 15 μm uncertainty in the location of the Li I 2s-2p peak, despite the ~80 μm MCP resolution and the ~10-15 Å 2s-2p line width[2]. These facts naturally motivate experimental tests of the measurement and analysis procedure.

Three different methods were used to verify the validity of the error analysis. The first method used a tunable laser diode to generate streaks at 6708 Å simultaneously on the eight channels of one of our multiplexed spectrographs. The premise of these calibrations is that the wavelength of the tunable laser diode streak can be measured at a sequence of 15-20 times on each of the eight systems, using an identical analysis procedure to the PBFA II experiments. The distribution of the measured wavelengths about the true wavelength should then have a width that corresponds to the ROBFIT error bars. The tunable laser diode width and intensity were adjusted to be similar to the PBFA II Li I 2s-2p line parameters. In addition, we superimposed continuum light at a variety of intensities, again to mimic the PBFA II experiment conditions. The distribution of the measured

wavelengths about the true wavelength was found to be Gaussian and the width of the distribution agreed with the width expected based on the error bars determined with the ROBFIT analysis. Table 1 shows the fraction of the points that lie within 1, 2, and 3 σ of the true wavelength, where 1, 2, and 3 σ refer to the size of the ROBFIT error bars for each individual measurement. The results from four laser diode calibrations using different signal levels are averaged in Table 1, along with the ideal fractions if the analysis works perfectly. The table shows that the calibrations generated good agreement between the ROBFIT error bars and the measured distributions, although in some cases the ROBFIT error bars were about 20% too small. The latter calibrations corresponded to lower injected signal levels. The conclusion is that our measurement and analysis technique results in error bars that are accurate to better than 20%.

The accuracy of our measurement / analysis method was also tested using PBFA II null tests. These tests were designed to record emission from the PBFA II gap on multiple systems, taking steps to render the Stark shift of the light injected into each channel equal. The setup for these experiments is shown in Figure 6. The idea is to collect light in fibers from several spatial locations in the diode, just as in a normal PBFA II experiment designed to measure the field. The light was then injected into a larger-diameter fiber (400 μm). The light mixes in the 400 μm fiber so that individual 100 μm fibers connected to the output all carry light with the same time-dependent Stark shift. The mixed light was then injected into six channels of a multiplexed streaked spectrograph for recording. Losses in the mixing process reduced the signals below that normally achieved and the streak camera gain had to be increased by about a factor of 2.2. The uncertainties in the measured PBFA II field are about $\pm$ 8%, significantly larger than on a normal PBFA II experiment because of the low signal levels. In order to evaluate whether the error bars from our

analysis are an accurate representation of the true uncertainty, we first compute the weighted average Stark shift from the six systems at each time step. Then the number of points that differ from the weighted average by more than 1, 2, and 3 σ was tallied, in a similar manner to our analysis of the laser diode null tests. The average over four PBFA II null experiments are shown in Table 1. As for the laser diode calibrations, the statistics generally agree with the ideal distribution, but the error bars are too low by 20% in some cases.

Perhaps the most powerful test of the accuracy of our error analysis method is actual PBFA II experiments in which the electric field was determined to be uniform. Such experiments are compelling because there is no difference between the experimental conditions or analysis in these measurements and the conditions where we measure a non-uniform field. These experiments use a line-of-sight arrangement similar to Figure 1 to measure the azimuthal uniformity as a function of radius. A statistically-significant azimuthal non-uniformity in the field is typically measured in these experiments at 5.5 mm and possibly at 3.1 mm from the anode. However, the field measured 0.7 mm from the anode was azimuthally uniform in all experiments. Thus, we can examine the distribution of the near-anode measurements about their mean as a way of evaluating the validity of the error bars determined with ROBFIT. Each experiment measured the field at 15 time steps and, if our error bars are an accurate representation of the uncertainty and the true field is the mean of the measurements, we expect 68% of the measurements to differ from the mean by less than 1σ. The actual tally of the measurements for a typical experiment is shown in Table 1. The conclusion from this analysis is that the error analysis is conservative, since a larger fraction of the data lies within 1, 2, and 3 σ of the mean than expected for an ideal Gaussian distribution. The difference between this result and the null tests may be due to un-intentionally-introduced extra-

neous noise sources in the null tests.

V. Results

The measurements and analysis described above enable the construction of a two-dimensional time-resolved map of the electric field magnitude in the ion diode acceleration gap. An example of the result obtained averaging over a 4 nsec interval in the middle of the power pulse is shown in Figure 7. The evolution of the data with time can be displayed as a 2-D movie, or as a sequence of radial or azimuthal plots. As described in References 1,3, & 5, the data can be used to determine the evolution of the charged particle density distributions. This information can then be used to evaluate and improve understanding of the complex plasma and atomic physics existing in the diode gap. The understanding can be improved by comparison with simulations or expectations based on analytic models[17]. Alternatively, as more data is acquired, an experimentally-based picture of diode operation can be constructed.

The present method that relies on naturally-occurring self-emission from the AK gap is powerful, but it also has certain limitations. For example, we integrate along a line of sight that may include variations in the field being measured, and measurements on the cathode side of the gap are inhibited because of the time that elapses before the charge-exchange neutrals arrive there. In addition, while the Li I 2s-2p transition is admirably suited to measuring 3-10 MV/cm fields, it is less sensitive to the lower fields characteristic of the virtual cathode location. These limitations can be largely removed by employing an active spectroscopy probe (ASP) technique. This involves injecting a localized Alkali-atom atomic beam into the diode, exciting it with laser induced fluo-

rescence, then recording the emission with our 2-D time-resolved spectroscopy system. The localization of the injected beam and the excitation by a controlled tunable laser provides three-dimensional space resolution and the low Doppler broadening of the neutral atoms should enable measurements of the magnetic field, in addition to providing higher-accuracy electric fields. This is similar to methods used to probe magnetic fusion devices, but it requires higher atom densities because of the need for ~1 nsec time resolution and the need to probe ~1-5 mm^3 volumes. Prior measurements[18] using a photomultiplier tube and bandpass filter detection system in a low-power electron beam diode indicate that this a promising technique. The requirements for successful ASP measurements are localized introduction of a suitable neutral atom beam without impacting the physics of the acceleration gap, while overcoming the difficulties associated with experiments performed on 20 TW 40-nsec-pulse accelerators. We intend to use Na in our first experiments since the 3s-3p resonance transitions are easily excited and observed, while the Stark shifts are amenable to measurements of electric fields in the 0.5-10 MV/cm range. We estimate the required density is about Benchtop experiments have verified that a 5 x 10^{12} cm^{-3} sodium density is readily produced using laser-ablation methods[19] and a mock-up of an accelerator experiment shows that this density provides an excellent signal-to-noise ratio. Work is in progress to measure plasma or other contaminant species that might accompany the desired neutral atom beam. We anticpate that these ASP measurements will enable un-ambigous testing of many fundamental diode-physics concepts, leading to progress in understanding and improving ion beam intensity.

Acknowledgment
We would like to thank P.M. Baca for technical assistance. We are also grateful to Y. Maron for many useful discussions and to D.L. Cook, R.J. Leeper, and J.P. Quintenz for continuous support and encouragement. This work was supported by the U.S. Department of Energy under contract No. DE-AC04-94AL85000.

Table Caption

Table 1. Evaluation of error bar analysis. The percent of data points within 1, 2, and 3 σ of the mean are compared with the expected percentages for Gaussian statistics (shown in perentheses). Results from two calibrations and from three distance relative to the PBFA II anode are shown.

Figure Captions

Figure 1. Schematic diagram of the cylindrically symmetric, biconic PBFA II ion diode. Space-resolved emission from the acceleration gap between the anode and virtual cathode (VC) is collected using a two-D fiber optic array.

Figure 2. Spectrograph mutiplexing conceptual diagram. We inject light on fiber optics that are displaced relative to the nominal entrance slit, resulting in output spectra that are also displaced. Multiple fiber channels are recorded by using a bandpass filter to eliminate the spectral overlap. The 1-m Czerny-turner spectrograph employs a 90 degree flat entrance mirror (M) and aspheric collimating and focussing mirrors (AM).

Figure 3. Measured properties of the multiplexed spectrograph. The fwhm values and the relative sensitivity are shown as a function of input fiber displacement in graphs a and b, respectively.

Figure 4. Multiplexed streaked spectrum from a PBFA II experiment. The eight Li I 2s-2p features correspond to fiber channels viewing eight different spatial positions in the diode acceleration gap.

Figure 5. Calibration data verifying Gaussian statistics. The top graph (a) shows the signal-to-noise ratio as a function of the signal for two MCP gain settings that differ by a factor of 2.1, along with the linear relation expected for Gaussian statistics. The bottom graphs (b) show that the distribution of the calibration data is Gaussian for moderate signal intensities (left plot) and that the distribution is Poisson-like when the signal is small (right hand plot).

Figure 6. Setup for PBFA II null tests.

Figure 7. Two-dimensional map of the electric field magnitude at a single time from PBFA II experiment # 6740. The anode is located at radius = 0. The variations with azimuth indicate deviations from ideal-diode behavior.

References

1. J.E. Bailey et al., *Phys. Rev. Lett.* 74,1771 (1995).
2. A.B. Filuk etal., submitted to Phys. Rev. Lett., 1996.
3. Y. Maron, M.D. Coleman, D.A. Hammer, and H.S. Peng, *Phys. Rev. Lett.* 57, 699 (1986), *Phys. Rev. A.* 36, 2818 (1987).
4. T.D. Pointon et.al., *Phys. Plasmas* 1, 429 (1994).
5. J.E. Bailey et al., Laser and Particle Beams, to be published (1996).
6. D.J. Johnson et. al., *J. Appl. Phys.* 53, 4579 (1982) and *Proc. 7th IEEE Pulsed Power Conf.* Monterey, CA, 1989, ed. by R. White and B.H. Bernstein, p. 944.
7. T.A. Mehlhorn, in *Proc. of 10th Int. Conf. on High Power Particle Beams*, San Diego, CA., NTIS # PB95-144317, p. 53 (1994).
8. J. Bailey, A.L. Carlson, R.L. Morrison, and Y. Maron, *Rev. Sci. Instrum.* 61, 3075 (1990) 4. S.A. Slutz, D.B. Seidel, and R.S. Coats, *J. Appl. Phys.* 59, 11 (1986).
9. N. Hawkes and N. Peacock, Rev. Sci. Instrum. 63, 5164 (1992).
10. R.P. Drake et al., Phys. Rev. Lett. 74, 3157 (1995), and references theirin.
11. Barr Assoc.,
12. Mcpherson, 530 Main St., Acton, Mass., 01720 .
13. R.J. Hertel, SPIE Vol. 1155, 332 (1989).
14. R.L. Coldwell and G.J. Bamford, *The,Theory and Operation of Spectral Analysis Using Robfit*, AIP, New York, (1991).
15. P.R. Bevington and D.K. Robinson, *Data Reduction and Error Analysis for the Physical Sciences*, McGraw Hill, New York, (1992).
16. K. McKammon et al., SPIE Vol. 1346, 398 (1990).
17. M.P. Desjarlais, *Phys. Rev. Lett.* 59, 2295 (1987).
18. B.A. Knyazev et al., in *Proc. of 9th Int. Conf. on High Power Particle Beams*, Washington, D.C.., NTIS # PB92-206168, p. 1043 (1992).
19. J.F. Friichtenicht, Rev. Sci. Instrum. 45, 51 (1974).

% of points within:	laser diode tests	PBFA *null* tests	PBFA experiment #6411		
			0.7 mm	3.1 mm	5.5 mm
1σ (68.3%)	62.7%	62.7%	97 %	71 %	38 %
2σ (95.4%)	92.7	90.7	100	94	75
3σ (99.7%)	97.7	99.3	100	100	88

Table 1

Figure 1

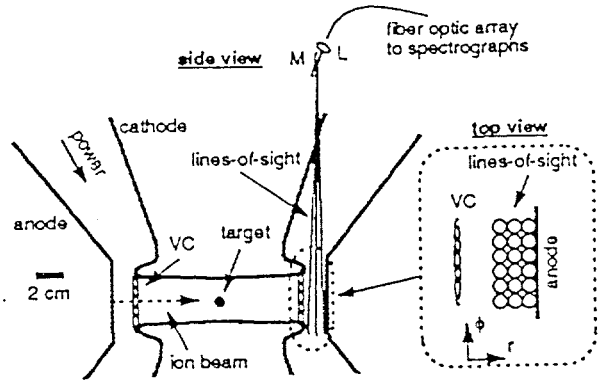
fiber optic array
to spectrographs
side view
M
L
cathode
power
lines-of-sight
anode
VC
target
2 cm
ion beam
top view
lines-of-sight
VC
anode
ϕ
r

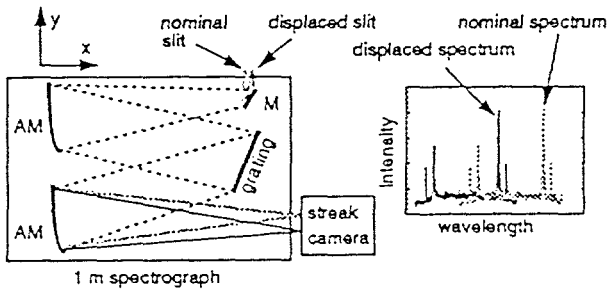
y
x
nominal slit
displaced slit
nominal spectrum
displaced spectrum
M
AM
AM
Grating
streak camera
1 m spectrograph
Intonelty
wavelength

Figure 2

reduce 5%

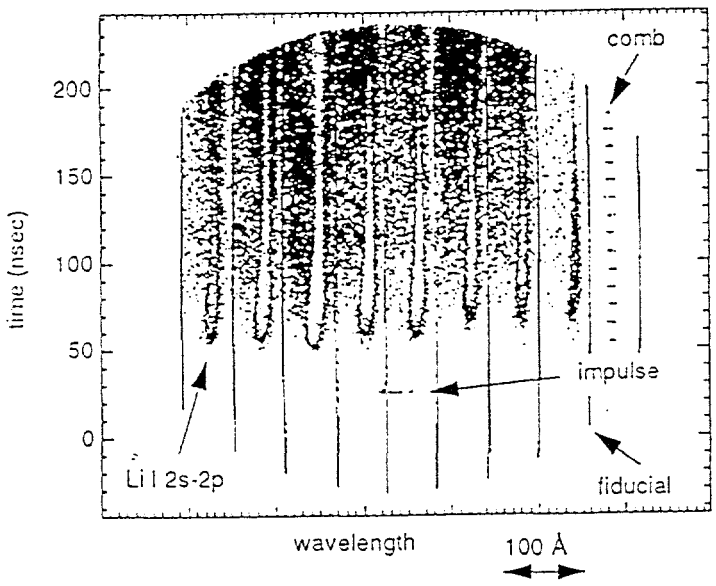

Figure 4

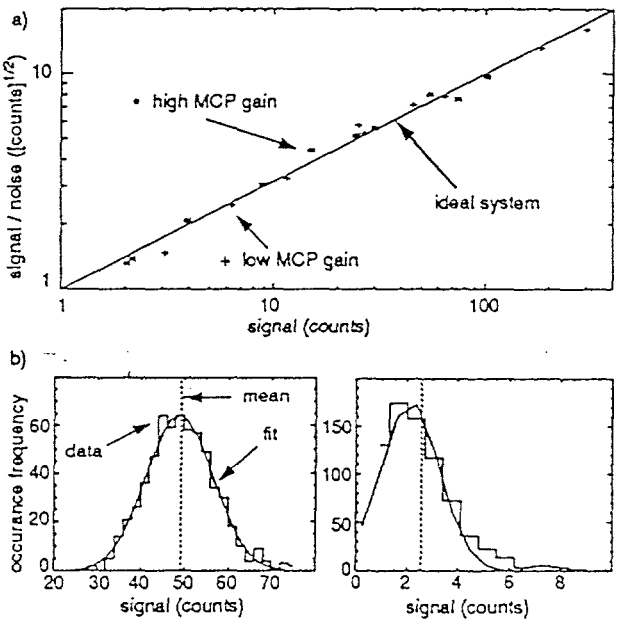
a)
signal / noise ([counts]^1/2)
10
1
high MCP gain
ideal system
low MCP gain
1
10
100
signal (counts)
b)
occurance frequency
mean
data
fit
60
40
20
0
20 30 40 50 60 70
signal (counts)
150
100
50
0
0 2 4 6 8
signal (counts)

Figure 5

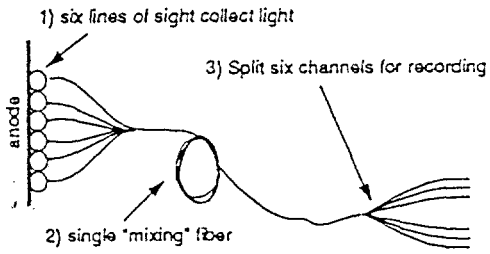
1) six lines of sight collect light
3) Split six channels for recording
anode
2) single "mixing" fiber

Figure 6

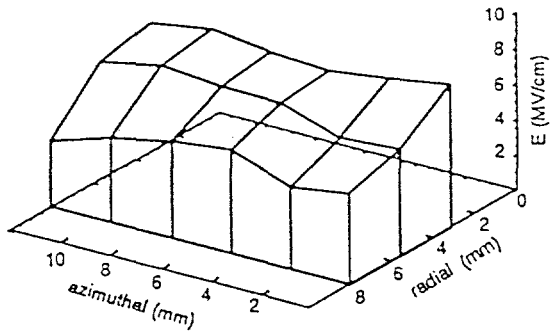

Figure 7